Scale-space flow for end-to-end optimized video compression

Eirikur Agustsson, David Minnen, Nick Johnston, Johannes Ballé, Sung Jin Hwang, George Toderici
Google Research, Perception Team
{eirikur, dminnen, nickj, jballe, sjhwang, gtoderici}@google.com

Abstract

Despite considerable progress on end-to-end optimized deep networks for image compression, video coding remains a challenging task. Recently proposed methods for learned video compression use optical flow and bilinear warping for motion compensation and show competitive rate-distortion performance relative to hand-engineered codecs like H.264 and HEVC. However, these learning-based methods rely on complex architectures and training schemes including the use of pre-trained optical flow networks, disjoint training of sub-networks, adaptive rate control, and buffering intermediate reconstructions to disk during training. In this paper, we show that a generalized warping operator that better handles common failure cases, e.g. disocclusions and fast motion, can provide competitive compression results with a greatly simplified model and training procedure. Specifically, we propose scale-space flow, an intuitive generalization of 2D optical flow that adds a scale parameter to allow the network to better model uncertainty. Our experiments show that a low-latency video compression model (no B-frames) using scale-space flow for motion compensation can outperform analogous state-of-the art learned video compression models while being trained using a much simpler procedure and without any pre-trained optical flow networks.

1. Introduction

Recently, there has been significant progress in the area of end-to-end optimized image compression, which went from barely matching JPEG [30], to methods such as [7, 23, 5] that can outperform the best hand-engineered codecs when evaluated in terms of multi-scale structural similarity (MS-SSIM) [33], PSNR, and according to subjective quality from user studies. While this is very encouraging, over 60% of downstream internet traffic currently consists of *video streaming* data [1], which means that in order to maximize impact on bandwidth reduction, researchers should focus on video compression.

Since the area of neural video compression is in early stages, it is not yet clear which network architectures are most effective for which application scenario. We can roughly categorize the existing research methods into the following three categories:

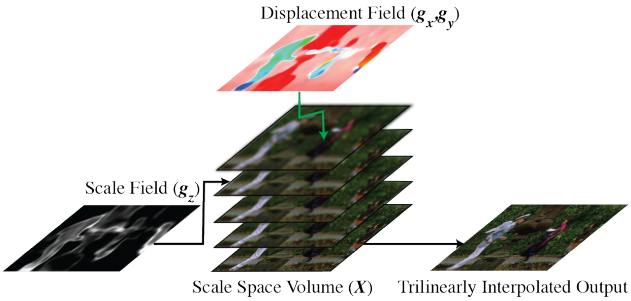

Figure 1. Our proposed Scale-Space Warping module: From the source image $\mathbf{x}$ we construct a fixed-resolution scale space volume $\mathbf{X}$. In contrast to bilinear warping, where the warped output is sampled directly from the source image using a 2-D displacement field $(\mathbf{f}_x, \mathbf{f}_y)$, we tri-linearly sample from the 3-D volume using a 3-D displacements+scale field $(\mathbf{g}_x, \mathbf{g}_y, \mathbf{g}_z)$. The additional scale field gives a continuous (and differentiable) knob that can be used to adaptively blur the source image during the warping step in regions where the warp is not a good prediction of the desired target image.

1) *3D autoencoders*: This is a natural extension of the work done for learned image compression, and [24] demonstrated that representing the video using spatiotemporal transformations alone does not lead to better performance compared to standard methods. However, when combined with temporally conditioned entropy models [16], such methods can perform on par with standard methods in terms of MS-SSIM.

2) *Frame interpolation methods*: It is natural to use neural networks to interpolate between frames in a video and then encode the residuals [35, 15]. This approach is commonly used in standard video coding (called "bidirectional prediction" or "B-frame coding") [34], but has the disadvantage that it is generally not suitable for low-latency streaming environments since such methods need information "from the future" to decode each B-frame. However,

im standard codecs, the use of B-frames typically provides the best rate-distortion (RD) performance when low-latency decoding is not required.

3) *Motion compensation via optical flow* [21, 27] is based on estimating and compressing optical flow which is applied with bilinear warping on the previously decoded frames to obtain a prediction of the frame currently being encoded. The residual error is then separately compressed to reduce total distortion and minimize temporal error accumulation. Recently published methods [21, 27] in this setting achieve compression that outperforms H.264 in terms of PSNR and HEVC in terms of MS-SSIM. However, these methods rely on complex architectures and training schemes, such as pre-trained optical flow networks [21], disjoint training of sub-networks [27, 21], adaptive rate control during encoding [27] and buffering intermediate reconstructions to disk during training [21].

Our research focuses on the last class of approaches, since it provides a good balance between rate-distortion performance and applicability to low-latency video streaming systems. However, we argue that using pre-trained optical flow networks[21] and bilinear warping[21, 27] may not be ideal for motion compensation:

1. Flow estimation needs to solve the *aperture problem*, which is not an issue for compression, so the model needlessly solves a harder problem than necessary. Moreover, optical flow networks aim to minimize motion vector error, while compression seeks to minimize a compromise between the bitrate necessary to encode the residual error and the distortion (i.e., reconstruction error).

2. The need to rely on existing optical flow network architectures thus potentially adds unnecessary constraints or complexity to the design of the compression networks.

3. Good optical flow performance requires a supervised training stage, which relies on annotated flow data, complicates the training procedure, and limits the domains of applicability.

4. Unlike standard video codecs that use motion compensation vectors, optical flow is dense, which means that every pixel is warped. Since there is no concept of "not using" a flow prediction, unnecessarily large residuals are expected in the case of disocclusions.

In this paper, we propose a generalization of optical flow and bilinear warping to *scale-space flow* and *scale-space warping* (see Figure 1), where a *scale field* is added as a third dimension to the typical spatial flow field. This per-location scale parameter allows the warping operation to better handle difficult cases and more gracefully degrade when no flow-based prediction is possible. The scale dimension acts as a differentiable "knob" that allows the model to adaptively blur the source content before warping, based on how well it predicts the next frame. Intuitively, this should lead to a smaller intermediate residual error and, in turn, to a more compressible residual since the model won't need to spend as many bits to "undo errors" introduced by the warping step.

Furthermore, we show that a scale-space warping operation integrated into a simple low-latency compression pipeline (depicted in Figure 2) can yield rate-distortion results outperforming recent state-of-the-art learning-based methods. Specifically, for equal PSNR, our method provides an average Bjøntegaard Delta (BD) rate reduction [11] of 13.4% compared to [21] and a savings of 42.9% over [35], while we see a 30.3% savings over [16] for equal MS-SSIM (see Section 5 for a detailed evaluation). Compared to prior approaches for flow-based motion compensation [21, 27], our system is significantly simpler since we do not need to separately estimate flow or use pre-trained networks. To achieve this, we do not need to make use of advanced training or encoding strategies such as buffering reconstructions [21] or spatially adaptive rate control [27].

Our ablation studies show (see Section 5) that compared to bilinear warping, the proposed scale-space warping significantly improves the rate-distortion performance with gains of more than 1dB at some bitrates.

In summary, our contributions are the following:

(i) We propose a scale space flow and warping, an intuitive generalization to flow + bilinear warping that reduces the need for complex residuals in failure cases.

(ii) Combined with a simple architecture and training procedure, we are able to train our model end-to-end from scratch, and the network learns to do motion compensation without utilizing any pre-trained optical flow networks.

(iii) Our experiment show that such a system leads outperforms recent state-of-the-art methods such as [21, 16], while our ablations show the same system trained for flow and bilinear warping performs significantly worse.

2. Related Work

Image Compression Recent image compression works [6, 9, 29, 4, 26, 7, 22, 5] have shown significant progress in terms of rate-distortion performance compared to standard codecs such as JPEG [31], JPEG2000 [18] and [10].

The most current state-of-the-art architectures [36, 13, 23] build on the hyperprior based system of [7], with improvements with autoregressive context models [23] and multi-rate training [13].

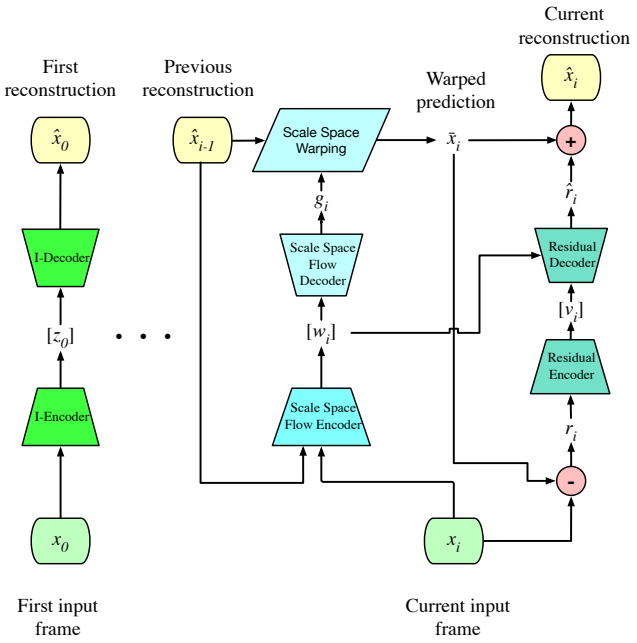

Figure 2. Overview of our end-to-end optimized, low-latency compression system: 1) the scale-space flow is jointly estimated and encoded to a quantized latent, $[w_i]$; 2) the previous reconstruction, $\hat{x}_{i-1}$, is scale-space warped using the decoded scale-space flow field, g_i, yielding the warped prediction, $\bar{x}_i$; 3) the remaining residual, $r_i = x_i - \bar{x}_i$, is encoded to a quantized latent, $[v_i]$, and its decoded version, $\hat{r}_i$, is added to the warped prediction giving the final reconstruction, $\hat{x}_i = \bar{x}_i + \hat{r}_i$. All of the encoder & decoder networks are simple four layer CNNs that are trained jointly after random initialization.

In this work, we consider these works foundational building blocks that we aim to apply into the video compression domain.

Standard Video Compression There is a long history of progress for standard video compression, with codecs progressively improving over the years, from H.263 [14], to H.264 [28] and more recently HEVC [3], so far roughly doubling bitrate savings with each generation. The methods provide valuable strong baselines to assess the performance of learned video compression methods, in particular [3] which remains a strong competitor to state-of-the-art learned video models.

Learned Video Compression As mentioned above, recent work on learned video compression roughly falls into three categories, of which motion compensation via optical flow is most related to our work. The architecture we adopt can be viewed as a greatly simplified version of the method of [21], which uses a pre-trained flow estimation network [25] combined with a flow compression module. In contrast, we directly learn the motion estimation module from scratch (see 'Scale Space Flow Encoder' in Figure 2) which jointly estimates and encodes the motion from the current input frame and previous reconstruction.

The training process of [21] happens in disjoint steps: the I-frame model is first trained and then the P-frame model, which only sees one frame at a time. To ensure the P-frame model can handle its own outputs as inputs, reconstructions of the P-frame model are buffered to disk during training and fed to the model. This complicates the training process and means that the P-frame model is trained using 'stale' previous reconstructions from an older version of the model. In contrast, we jointly train the I-frame and P-frame models together from scratch, unrolling it over multiple frames during training, which greatly simplifies the training procedure.

Uncertainty estimates for optical flow The scale parameter of our proposed scale-space flow (see Figure 1) can be interpreted as an 'uncertainty parameter' in the sense that it is natural to use a high scale value in regions where it is not feasible to obtain a good prediction via warping. While prior work on supervised optical flow studied how to integrate uncertainty into the predictions of flow estimation networks (see [17] for overview), such methods operate in the supervised setting: i.e. they predict the uncertainty in the prediction of *ground truth* flow. In contrast, this work focuses on generalizing the flow + warping operation so that the warped result forms a good prediction – irrespective of the relationship between the displacement field and ground truth flow.

3. Method

3.1. Scale-space flow

Our proposed scale-space flow (see Figure 1 for overview) generalizes flow and bilinear warping to also incorporate Gaussian blurring.

Given an image $\mathbf{x}$ with a spatial shape of $H \times W$ and a flow field $\mathbf{f} = (\mathbf{f}_x, \mathbf{f}_y)$, the bilinear warping of $\mathbf{x}$ by $\mathbf{f}$ is denoted as

$$\begin{aligned} &\mathbf{x}' := \text{Bilinear-Warp}(\mathbf{x}, \mathbf{f}) \qquad \text{s.t.} \\ &\mathbf{x}'[x, y] = \mathbf{x}[x + \mathbf{f}_x[x, y], y + \mathbf{f}_y[x, y]] \end{aligned} \tag{1}$$

where $\mathbf{x}[x, y]$ denotes sampling the image $\mathbf{x}$ at (continuous) coordinates (x, y) using bilinear interpolation. We refer to the flow channels $\mathbf{f}_x, \mathbf{f}_y \in \mathbb{R}^{H \times W}$ as the x- and y-displacement fields of the flow $\mathbf{f}$.

For scale-space warping, we construct a fixed-resolution scale-space volume $X = [\mathbf{x}, \mathbf{x} * G(\sigma_0), \mathbf{x} * G(2\sigma_0), \cdots, \mathbf{x} * G(2^M \sigma_0)]$, where $\mathbf{x} * G(\sigma)$ denotes the convolution of $\mathbf{x}$ with a Gaussian kernel with scale σ. We use 3-D indexing $\mathbf{X}[x, y, z]$ to denote a sample taken from a spatial location (x, y) with a scale level z.

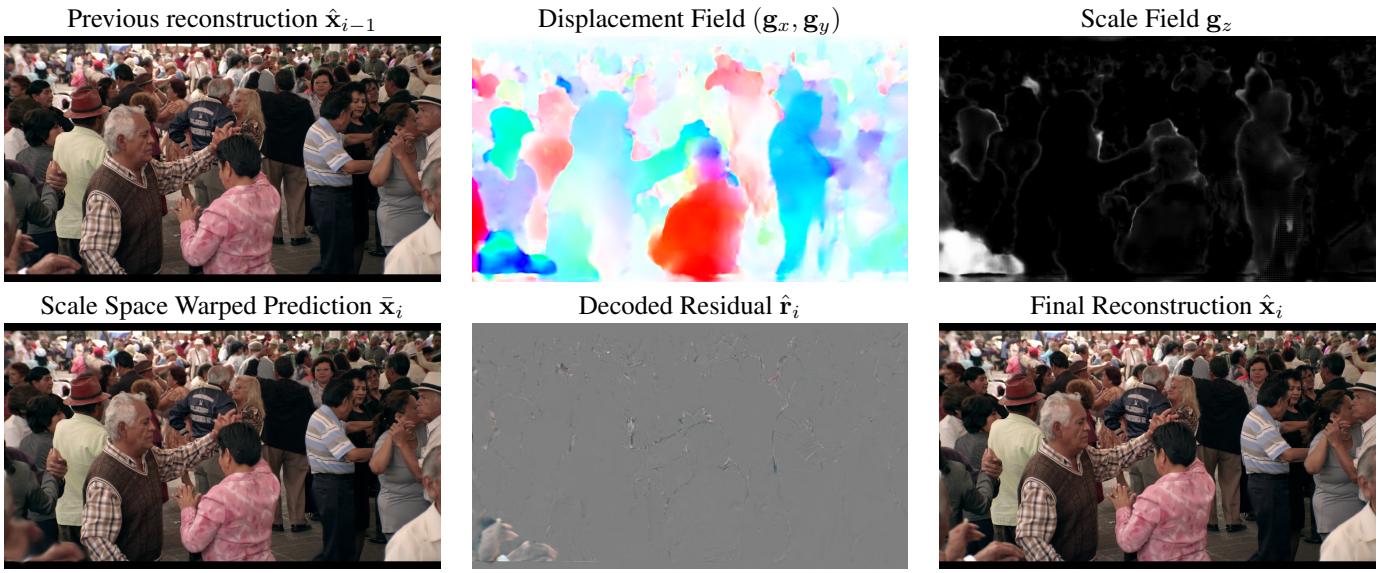

Figure 3. Visualization of the the internals of our model. The network learns to predict spatial flow even for a crowded scene. Note how the scale parameter increases around the boundaries of the people where warping is least likely to provide an accurate reconstruction. Similarly, in the bottom left corner of the image, the motion of the hands is not modeled well by warping so the network predicts a larger scale value that results in a blurrier intermediate reconstruction that ultimately helps minimize the global RD loss.

X represents a stack of progressively blurred versions of x with dimensions $H \times W \times M$, which we can sample at continuous coordinates (x, y, z) via trilinear interpolation.

We now define a scale-space flow field as a 3 channel field $\mathbf{g} := (\mathbf{g}_x, \mathbf{g}_y, \mathbf{g}_z)$, and the corresponding scale-space warp of the image $\mathbf{x}$ as

$$\begin{aligned} &\mathbf{x}' := \text{Scale-Space-Warp}(\mathbf{x}, \mathbf{g}) \qquad \text{s.t.} \\ &\mathbf{x}'[x, y] = \mathbf{X}[x + \mathbf{g}_x[x, y], y + \mathbf{g}_y[x, y], 0 + \mathbf{g}_z[x, y]] \end{aligned} \tag{2}$$

We refer to the newly introduced third flow channel $\mathbf{g}_z \in \mathbb{R}_+^{H \times W}$ as the scale-field of the scale-space flow $\mathbf{g}$.

We note that Scale-Space-Warp is strictly more general than both bilinear warping and Gaussian smoothing. In particular, for $\mathbf{g} = (\mathbf{g}_x, \mathbf{g}_y, \mathbf{g}_z)$:

- When $\mathbf{g}_z = 0$ we obtain bilinear warping as a special case:

$$\begin{aligned} &\text{Scale-Space-Warp}(\mathbf{x}, (\mathbf{g}_x, \mathbf{g}_y, \mathbf{0})) = \\ &\qquad \text{Bilinear-Warp}(\mathbf{x}, (\mathbf{g}_x, \mathbf{g}_y)) \end{aligned} \tag{3}$$

- When $\mathbf{g}_x = \mathbf{g}_y = 0$ and $\mathbf{g}_z = \log_2(\sigma/\sigma_0)$ for $\sigma > \sigma_0$ we recover Gaussian blur as a special case:

$$\text{Scale-Space-Warp}(\mathbf{x}, (0, 0, 1{+}\log_2(\sigma/\sigma_0)) \approx \mathbf{x} {*} G(\sigma), \tag{4}$$

  where equality holds if $\log_2(\sigma/\sigma_0) \in \{0, \cdot, M\}$.

Differentiability Since we use trilinear interpolation (across the 2+1 space and scale dimensions) for the Scale-Space-Warp operation, it is differentiable with respect to all the arguments $(\mathbf{x}, \mathbf{g}_x, \mathbf{g}_y, \mathbf{g}_z)$.

Complexity The additional complexity of Scale-Space-Warp as described above comes from having to construct the volume $\mathbf{X}$ as a stack of progressively blurred versions of the frame and the larger memory associated with storing it, which is linear in the number of scale levels N (which we set to $N = 5$ throughout our experiments). We chose this representation because it makes the implementation of trilinar warping very easy to implement. However, we note that one could technically replace $\mathbf{X}$ with a multi-scale pyramid where the image is decimated at each level, since the signal can be safely decimated after Gaussian filtering [20]. This would reduce the memory cost to a factor of $1{+}1/4{+}1/8{+}\cdots = 1.33$ but makes the implementation more complex, since it is no longer a matter of interpolating within a single $3D$ tensor, but rather within a stack of $2D$ tensors.

Reparameterization As mentioned above, the Gaussian kernel size as a function of the volume level is $[0, \sigma_0, 2\sigma_0, ..., 2^M\sigma_0]$, since the first level corresponds to the original image which hasn't been filtered. For a more natural parameterization, we observe that when tri-linearly interpolating a given (continuous) scale z that falls between scale levels $i \leq z < i + 1$, with corresponding Gaussian kernel sizes σ_a and σ_b, the effective kernel size of the equivalent linear filter (i.e. the standard deviation of the linear combination of the Gaussians) is $\sigma_z = \sqrt{(z - i)^2\sigma_a + (1 - z + i)\sigma_b^2}$. So given a desired

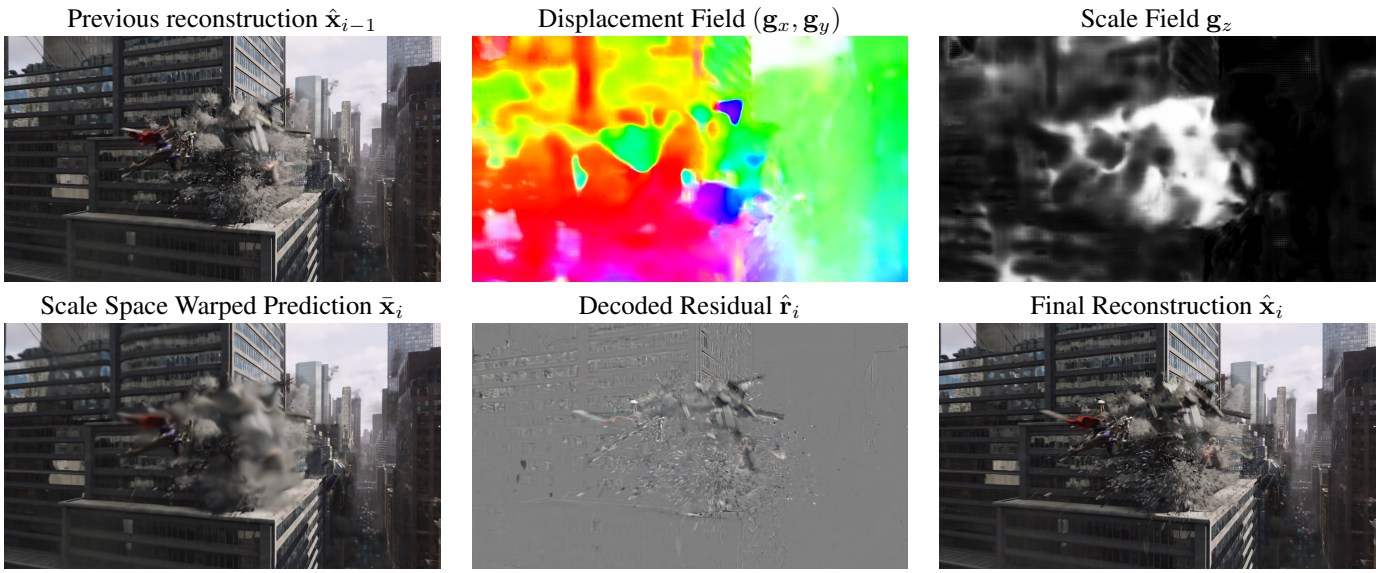

Figure 4. For this pair of frames, the camera motion is relatively well-modeled by the flow predictor, but the explosion in the center can not be modeled accurately by warping. To compensate, the network uses the scale field to blur the explosion and relies on the compressed residual to generate a high-quality reconstruction. Without the scale field, inaccurate warping can lead to a larger residual with a worse rate-distortion trade-off.

(continuous) kernel size $0 < \sigma_t < 2^M \sigma_0$, we can easily solve for the corresponding value of z. Thus, we use the more natural parameterization through σ_t when specifying or predicting the scale field (as done with a neural network in the next section).

Composition While we do not study multi-scale architectures in this paper, it is common practice to do so for optical flow estimation [25, 12], where the *compositionality* of bilinear warping is exploited: when warping with a (potentially upscaled) field $\mathbf{f}_1$ followed by $\mathbf{f}_2$, one can specify an equivalent field $\mathbf{f}_3$ that achieves the same in a single operation. We note that it would in principle also be possible to integrate scale-space warping into such architectures, since Gaussian filtering has such compositionality [20].

3.2. Compression Model

Our model is targeted for **low-latency scenarios**, which refers to the setting where only previous (decoded) frames are available when encoding (or decoding) a given image. In Figure 2, we give an overview of how scale-space warping can be integrated into such a compression architecture.

Given a sequence of frames $\mathbf{x}_0, \cdots, \mathbf{x}_N$ we encode the first (I) frame to a latent $\mathbf{z}_0$ which is quantized to integer values $[\mathbf{z}_0]$, obtaining a reconstruction $\hat{\mathbf{x}}_0$. Now, for a currently given (P-) frame $\mathbf{x}_i$, we use a single network to jointly estimate and encode (quantized) scale-space warp latents $[\mathbf{w}_i]$, from which we decode a scale-space flow $\mathbf{g}_i$. We then scale-space warp the previous reconstruction $\hat{\mathbf{x}}_{i-1}$ to obtain an estimate of the current frame $\bar{\mathbf{x}}_i$. Since the estimate $\bar{\mathbf{x}}_i$ will be imperfect, a second branch will encode the residual $\mathbf{r}_i = \mathbf{x}_i - \bar{\mathbf{x}}_i$ to a latent $[\mathbf{v}_i]$ and apply the decoded residual $\hat{\mathbf{r}}_i$ to obtain a final reconstruction $\hat{\mathbf{x}}_i = \bar{\mathbf{x}}_i + \hat{\mathbf{r}}_i$.

For each of the three latent types, $\mathbf{z}_0, \mathbf{v}_i, \mathbf{w}_i$ we use a separate hyperprior [23] to model the corresponding density (three in total) without the autoregressive component.

To summarize, we employ the autoencoder [23] architecture proposed for image compression for the purposes of I-frame compression, residual compression and scale space flow computation. This is different from previous work, which typically employed a specialized optical flow network.

3.3. Quantization and entropy estimation

While we generally adopt the approach of [9] to replace quantization with additive uniform noise to approximate Shannon cross entropy during training with differential cross entropy, we found that for the purpose of propagating "quantized" latents/residuals through further transformations, it was beneficial to use a straight-through estimator (i.e., quantize during training as well as evaluation, and substitute the gradient of the quantizer with the identity function for training). Our approach is thus a combination of the proposals in [9] and [29].

3.4. Loss

We optimize the whole system for the joint RD-loss unrolled over N frames.

$$\sum_{i=0}^{N-1} d(\mathbf{x}_i, \hat{\mathbf{x}}_i) + \lambda \left[H(\mathbf{z}_0) + \sum_{i=1}^{N-1} H(\mathbf{v}_i) + H(\mathbf{w}_i) \right], \quad (5)$$

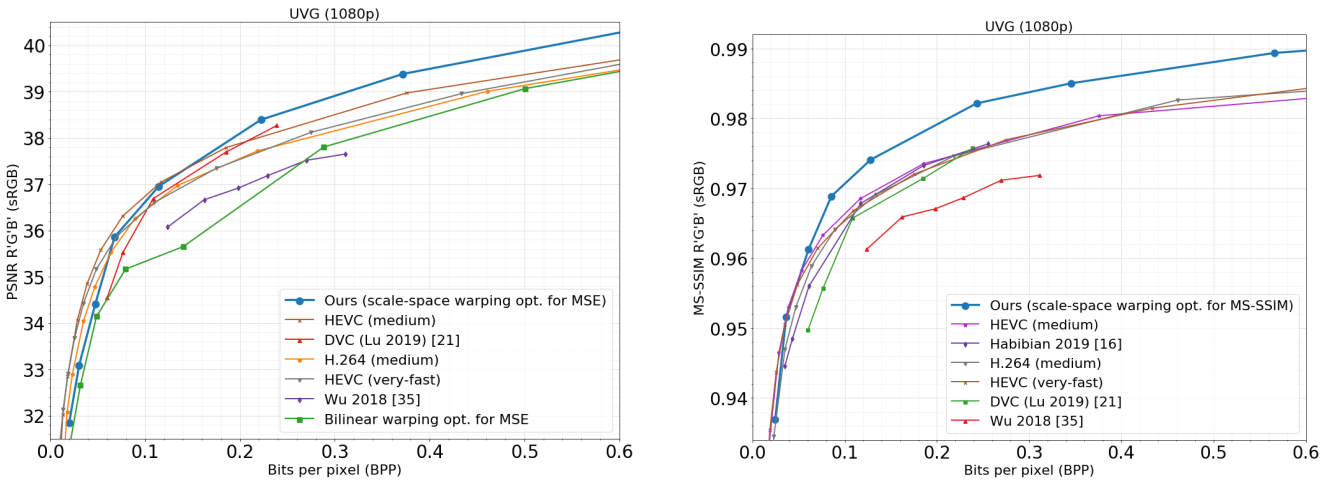

Figure 5. Rate-distortion comparison on the UVG dataset [2] using PSNR (*left*) and MS-SSIM (*right*). Our approach outperforms existing low-latency research models ([21, 35, 16]) at all bit rates for both metrics. Our method outperforms HEVC above 0.15 bpp for PSNR and above 0.05 bpp according to MS-SSIM.

where $H(\cdot)$ denotes the entropy estimate of the repective latent, including the side information extracted by its hyperprior (see [23] for details). This means that during training, the bitrate allocation between the image latent $\mathbf{z}_0$, the motion compensation latents $\mathbf{w}_i$ and the residual latents $\mathbf{v}_i$ are all automatically determined by the system.

Equation 5 does not contain any loss terms specific to optical flow such as warping losses or total variation regularization. Instead, our networks learn to perform motion compensation with the scale-space flow directly as a byproduct of minimizing the rate-distortion equation.

4. Experimental setup

Architecture Our system uses a simplified version of the architecture from the hyperprior image compression system [23] as a building block, using ReLU activations instead of GDN [8] (see Supplementary for full details). In particular, we used the encoder architecture of [7] for the 'I-Encoder', 'Scale Space Flow Encoder' and 'Residual Encoder', and the corresponding decoder architecture for 'I-Decoder', 'Scale Space Flow Decoder' and 'Residual Decoder' (Figure 2).

Training data The models were trained on video frames extracted from approx. 700,000 high definition (1920×1080) videos with a frame rate of 30Hz. From each video sequence, we extracted 60 consecutive frames, which were partitioned into temporal chunks of $N = 3$ frames. To reduce pre-existing compression artifacts, the chunks were then downsampled by a randomized factor averaging $\frac{2}{3}$, and randomly cropped to 256×256 or 384×384 pixels (see details below). These video fragments were then randomized, and batches of 8 fragments each were fed to the training algorithm.

Colorspace We train and evaluate our models in the sRGB colorspace. This is not ideal, because the native format for most video content is Y'CbCr with chroma subsampling, and the conversion to and from sRGB is not lossless. However, we adopt sRGB to facilitate comparison with almost all published work in neural video compression [35, 21, 16, 24, 15].

Trained models We optimized our model both for MSE and MS-SSIM using 9 rate points covering a bitrate range of 0.025 to 0.8 bpp. In particular, we used $\lambda = 0.01 \cdot 2^i$ for MSE and $\lambda = 10 \cdot 2^i$ for MS-SSIM, where $i = -3, \ldots, 5$. We refer to these models as 'Ours (scale-space warping opt. for MSE)' and 'Ours (scale-space warping opt. for MS-SSIM,' respectively. To measure the benefit of scale-space warping, we optimized 9 models for MSE in an identical fashion, with the only difference being the warp method (i.e. in Figure 2 we change Scale-Space-Warp to Bilinear-Warp and output a 2-channel flow $\mathbf{f}$ instead of the 3 channel scale-space flow $\mathbf{g}$ in the corresponding decoder). We refer to this model as 'Bilinear warping opt. for MSE.'

Training schedule For training we used the Adam[19] optimizer with a base learning rate of 10^{-4}, batch size of 8 and a crop size of 256 pixels. To further reduce training costs, we trained all models for an MSE loss for the first 1,000,000 steps (which could be shared across the MSE and MS-SSIM models), and then further trained the MS-SSIM models for 200,000 steps with the MS-SSIM loss. Finally, for all models we decayed the learning rate to 10^{-5} for 50,000 steps, increasing the crop size to 384×384 pixels at the same time.

Number of unrolled frames While training for $N = 9$ or $N = 12$ unrolled frarmes yielded good results for the ini-

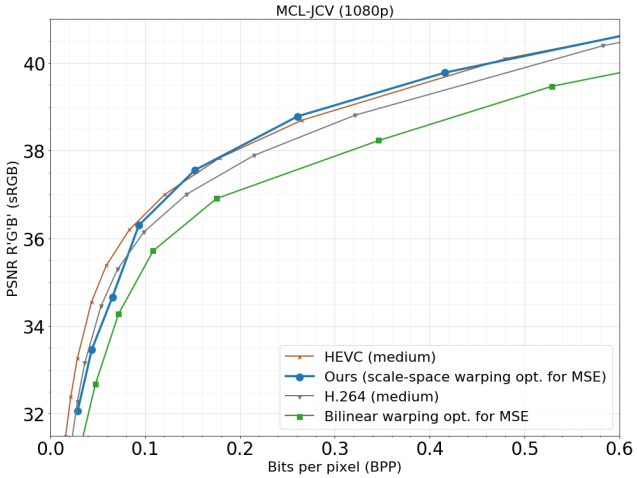

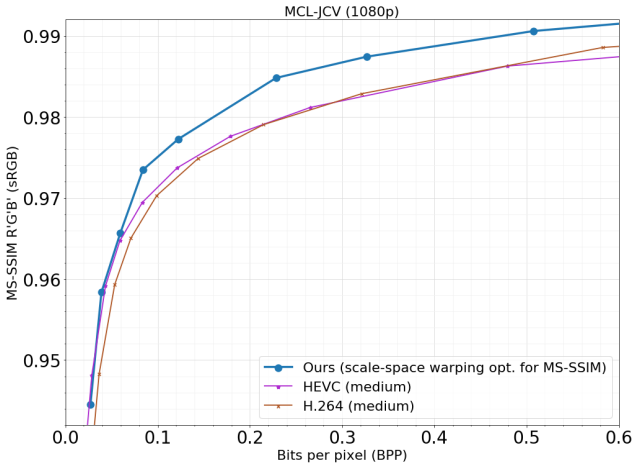

Figure 6. Rate-distortion comparison on the MCL-JCV dataset [32]. Our approach outperforms H.264 above 0.08 bpp on PSNR but has worse rate-distortion performance than HEVC. On MS-SSIM, however, our method outperforms H.264 at all bit rates and exceeds HEVC above 0.08 bpp. We believe the relatively poor PSNR results are due to the presence of several animated videos in the MCL-JCV dataset for which our model was not optimized (see Figure 8 for details).

tial models we explored, the training speed was too slow for practical experimentation with 1,000,000 training steps taking 30 days to train on a NVidia V100 GPU. We found that similar results could be obtained by training with $N = 3$ frames and without passing gradients from the I-frame reconstruction to the P-frame branch (to avoid the I-frame loss dominating the optimization). We trained all the models in this setting, which reduces the training time to approx. 4 days and allows for much faster experimentation.

Standard baselines and compared methods We evaluate the RD performance of our method and compare it with recently published learning-based methods [21, 16, 35] as well as standard codecs (H.264 [28] and HEVC [3]). We evaluate H.264 and HEVC using typical `ffmpeg` settings for low-latency mode, i.e. medium profile with B-frames disabled (see Supplementary for the full command line), and we refer to the results as *H.264 (medium)* and *HEVC (medium)* below. To ensure we perform an apples-to-apples comparison with recent methods, we also evaluate HEVC with the settings used in [21, 16, 35] to verify the baseline matches what is reported in those papers, which we refer to as *HEVC (very-fast)*.

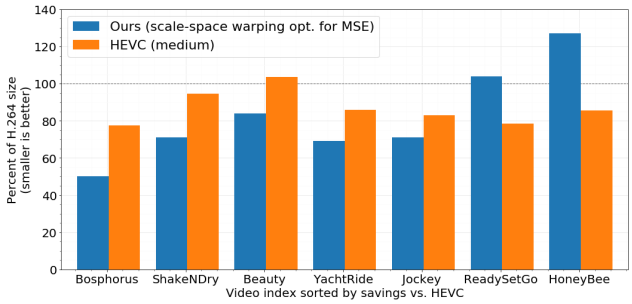

Figure 7. Rate savings for each video in the UVG dataset [2]. Values represent the file size relative to H.264 as estimated by BD rate for equal PSNR, e.g. an average rate savings of 25% yields a value of 75% (100% – 25%).

5. Results

Qualitative results In Figures 3 & 4, we visualize the internals of our models for input frames taken from two different evaluation videos. We observe that the model learns to compensate for complex motion in crowded scenes, predicting flow-like displacement fields while purely being trained for the rate-distortion objective in Eq. (5). When the motion is too complex to be captured by bilinear warping, the model utilizes the scale field to produce a simpler residual.

Quantitative results on the UVG dataset In Figure 5, we show the RD performance on the UVG dataset [2], both in terms of PSNR and MS-SSIM. For PSNR, our MSE-optimized model outperforms the recently introduced DVC method [21], which uses a much more complex architecture with a pre-trained multi-scale optical flow network for motion compensation. Furthermore, we outperform HEVC (`-preset very-fast`) at bitrates above ~0.07 bpp and exceed HEVC (`-preset medium`, the default setting) above ~0.15 bpp. When optimized for MS-SSIM, our model significantly outperforms all of the learning-based methods and H.264 over the entire range of bitrates, and its performance exceeds HEVC above ~0.05 bpp.

Quantitative results on the MCL-JCV dataset In Figure 6, we evaluate our model on the MCL-JCV dataset [32]. In terms of MS-SSIM, our MS-SSIM optimized model

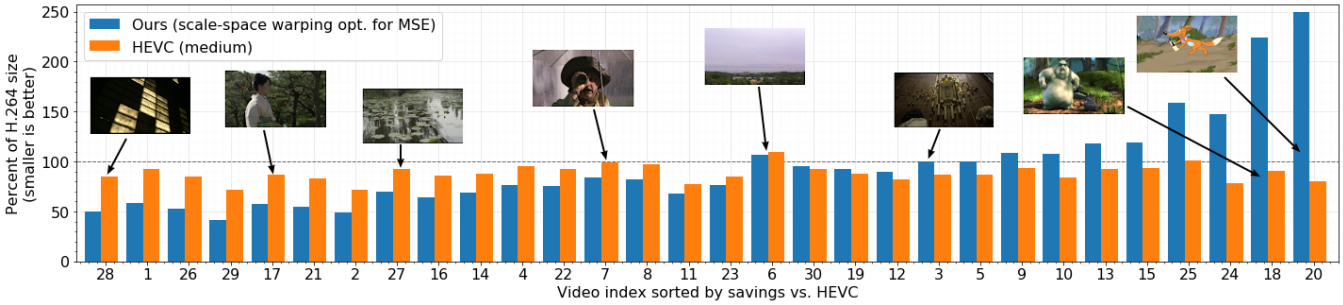

Figure 8. Rate savings for each video in the MCL-JCV dataset [32]. Values represent the file size relative to H.264 as estimated by BD rate for equal PSNR. Our method has smaller or equal file sizes than both H.264 and HEVC for most videos (21/30 and 17/30 respectively), but performs worst on animations (videos 20, 18, 24, and 25), which is not surprising since the training data primarily contains natural videos.

outperforms H.264 at all bit rates and exceed HEVC above ~0.075 bpp. However, when evaluated using PSNR, our MSE-optimized model only outperforms H.264 above ~0.08 bpp, and trails HEVC bitrates below 0.1bpp.

Per-Video level analysis on MCL-JCV In Figure 8, we compute the Bjøntegaard Delta (BD) rate reduction [11] for equal PSNR relative to H.264 [28] for each video in the MCL-JCV dataset. We then plot the relative size of each encoded video compared to H.264. For example, a BD rate savings of 15% means that the relative size is 85% (100% – 15%). By construction, the H.264 result is always 100.0%.

We can see that in terms of BD rate that compared to H.264, for a large majority of videos (21/30) we have smaller or equal file sizes than H.264. However, for a fraction of the videos (4/30) have more than 50% larger file sizes than H.264, of which two are more than double the size. The videos where our method is exceptionally challenged (videos 18, 20, 24, and 25) are all animations, and this could be explained by the lack of such videos in our training dataset, as well as the challenge of estimating motion for such videos that tend to have much less texture. Compared to HEVC, it is promising to see that we have significantly smaller file sizes for about half (17/30) of the videos, despite being in terms of PSNR our model is overall challenged against HEVC on MCL-JCV as shown in Figure 6 (*left*).

Bilinear warp vs Scale-Space warp Comparing our method with the (identically trained) "Bilinear warping" baseline, we find in Figures 5 & 6 that the performance gain of scale-space warping is significant both on the UVG and the MCL-JCV dataset, with a gap of 1dB for bitrates above 0.1bpp.

6. Discussion

In this paper, we proposed scale-space flow and scale-space warping as a generalization of flow and bilinear warping for use in the motion compensation step of learned video compression. Scale-space warping allows our network to better model regions which are poorly predicted with bilinear warping due to issues like disocclusion and fast or erratic motion.

We studied the scale-space warping operation in a simple low-latency motion compensation pipeline, without any pretrained optical flow or complex training or evaluation procedures. Our evaluation shows that it outperforms recent state-of-the-art learning-based methods [21, 16, 35] as well as the standard codecs H.264 and HEVC when evaluated using MS-SSIM.

While the field of learned video compression is still in its infancy, and the research community is still figuring out the best architectures, we believe scale-space warping provides a useful component and a novel and competitive direction for future model explorations. Future directions could include studying more complex architectures (including multi-scale models) and generalizations that use more than one previous frame for warping. Further research is also needed to improve generalization to animated videos and to intelligently place I-frames to better handle scene cuts and other abrupt changes.

References

[1] Report: Where Does the Majority of Internet Traffic Come From? https://www.ncta.com/whats-new/report-where-does-the-majority-of-internet-traffic-come. Accessed: 2019-11-12. 1

[2] Ultra video group test sequences. http://ultravideo.cs.tut.fi. 6, 7

[3] ITU-R rec. H.265 & ISO/IEC 23008-2: High efficiency video coding, 2013. 3, 7

[4] Eirikur Agustsson, Fabian Mentzer, Michael Tschannen, Lukas Cavigelli, Radu Timofte, Luca Benini, and Luc Van Gool. Soft-to-Hard Vector Quantization for End-to-End Learning Compressible Representations. In *NIPS*, 2017. 2

[5] Eirikur Agustsson, Michael Tschannen, Fabian Mentzer, Radu Timofte, and Luc Van Gool. Generative adversarial networks for extreme learned image compression. In *Proceedings of the IEEE International Conference on Computer Vision*, pages 221–231, 2019. 1, 2

[6] Johannes Ballé, Valero Laparra, and Eero P Simoncelli. End-to-end Optimized Image Compression. *ICLR*, 2016. 2

[7] Johannes Ballé, David Minnen, Saurabh Singh, Sung Jin Hwang, and Nick Johnston. Variational Image Compression with a Scale Hyperprior. *ICLR*, 2018. 1, 2, 6

[8] Johannes Ballé, Valero Laparra, and Eero P. Simoncelli. Density modeling of images using a generalized normalization transformation. *arXiv e-prints*, 2016. presented at the 4th Int. Conf. on Learning Representations. 6

[9] Johannes Ballé, Valero Laparra, and Eero P. Simoncelli. End-to-end optimized image compression. *arXiv e-prints*, 2017. presented at the 5th Int. Conf. on Learning Representations. 2, 5

[10] F. Bellard. BPG image format (http://bellard.org/bpg/). Accessed: 2017-01-30. 2

[11] Gisle Bjøntegaard. Calculation of average PSNR differences between RD-curves. Doc. VCEG-M33, ITU-T SG16/Q6 VCEG, Austin, TX, USA, Apr. 2001. 2, 8

[12] Jia-Ren Chang and Yong-Sheng Chen. Pyramid stereo matching network. In *Proceedings of the IEEE Conference on Computer Vision and Pattern Recognition*, pages 5410–5418, 2018. 5

[13] Yoojin Choi, Mostafa El-Khamy, and Jungwon Lee. Variable rate deep image compression with a conditional autoencoder. In *Proceedings of the IEEE International Conference on Computer Vision*, pages 3146–3154, 2019. 2

[14] Guy Cote, Berna Erol, Michael Gallant, and Faouzi Kossentini. H. 263+: Video coding at low bit rates. *IEEE Transactions on circuits and systems for video technology*, 8(7):849–866, 1998. 3

[15] Abdelaziz Djelouah, Joaquim Campos, Simone Schaub-Meyer, and Christopher Schroers. Neural inter-frame compression for video coding. In *Proceedings of the IEEE International Conference on Computer Vision*, pages 6421–6429, 2019. 1, 6

[16] Amirhossein Habibian, Ties van Rozendaal, Jakub M Tomczak, and Taco S Cohen. Video compression with rate-distortion autoencoders. In *Proceedings of the IEEE International Conference on Computer Vision*, pages 7033–7042, 2019. 1, 2, 6, 7, 8

[17] Eddy Ilg, Ozgun Cicek, Silvio Galesso, Aaron Klein, Osama Makansi, Frank Hutter, and Thomas Brox. Uncertainty estimates and multi-hypotheses networks for optical flow. In *Proceedings of the European Conference on Computer Vision (ECCV)*, pages 652–667, 2018. 3

[18] Information technology–JPEG 2000 image coding system. Standard, International Organization for Standardization, Geneva, CH, Dec. 2000. 2

[19] Diederik P Kingma and Jimmy Ba. Adam: A method for stochastic optimization. *arXiv preprint arXiv:1412.6980*, 2014. 6

[20] Tony Lindeberg. *Scale-space theory in computer vision*, volume 256. Springer Science & Business Media, 2013. 4, 5

[21] Guo Lu, Wanli Ouyang, Dong Xu, Xiaoyun Zhang, Chunlei Cai, and Zhiyong Gao. DVC: An end-to-end deep video compression framework. In *Proceedings of the IEEE Conference on Computer Vision and Pattern Recognition*, pages 11006–11015, 2019. 2, 3, 6, 7, 8

[22] Fabian Mentzer, Eirikur Agustsson, Michael Tschannen, Radu Timofte, and Luc Van Gool. Conditional probability models for deep image compression. In *2018 IEEE Conf. on Computer Vision and Pattern Recognition (CVPR)*, 2018. 2

[23] David Minnen, Johannes Ballé, and George D Toderici. Joint Autoregressive and Hierarchical Priors for Learned Image Compression. In *NeurIPS*. 2018. 1, 2, 5, 6

[24] Jorge Pessoa, Helena Aidos, Pedro Tomás, and Mário AT Figueiredo. End-to-end learning of video compression using spatio-temporal autoencoders. 2018. 1, 6

[25] Anurag Ranjan and Michael J Black. Optical flow estimation using a spatial pyramid network. In *Proceedings of the IEEE Conference on Computer Vision and Pattern Recognition*, pages 4161–4170, 2017. 3, 5

[26] Oren Rippel and Lubomir Bourdev. Real-time adaptive image compression. In *Proc. of Machine Learning Research*, volume 70, pages 2922–2930, 2017. 2

[27] Oren Rippel, Sanjay Nair, Carissa Lew, Steve Branson, Alexander G Anderson, and Lubomir Bourdev. Learned video compression. In *Proc. ICCV*, pages 3454–3463, 2019. 2

[28] Heiko Schwarz, Detlev Marpe, and Thomas Wiegand. Overview of the scalable video coding extension of the h. 264/avc standard. *To appear in IEEE Transactions on Circuits and Systems for Video Technology*, page 1, 2007. 3, 7, 8

[29] Lucas Theis, Wenzhe Shi, Andrew Cunningham, and Ferenc Huszár. Lossy image compression with compressive autoencoders. 2017. presented at the 5th Int. Conf. on Learning Representations. 2, 5

[30] George Toderici, Damien Vincent, Nick Johnston, Sung Jin Hwang, David Minnen, Joel Shor, and Michele Covell. Full resolution image compression with recurrent neural networks. In *2017 IEEE Conf. on Computer Vision and Pattern Recognition (CVPR)*, 2017. 1

[31] Gregory K. Wallace. The jpeg still picture compression standard. *Communications of the ACM*, pages 30–44, 1991. 2

[32] Haiqiang Wang, Weihao Gan, Sudeng Hu, Joe Yuchieh Lin, Lina Jin, Longguang Song, Ping Wang, Ioannis Katsavounidis, Anne Aaron, and C-C Jay Kuo. Mcl-jcv: a jnd-based h. 264/avc video quality assessment dataset. In *2016 IEEE International Conference on Image Processing (ICIP)*, pages 1509–1513. IEEE, 2016. 7, 8

[33] Zhou Wang, Eero P Simoncelli, and Alan C Bovik. Multiscale structural similarity for image quality assessment. In *Signals, Systems and Computers, 2004. Conference Record of the Thirty-Seventh Asilomar Conference on*, volume 2, pages 1398–1402. IEEE, 2003. 1

[34] wikipedia. Video compression picture types, 2019g. [Online; accessed 15 November 2019]. 1

[35] Chao-Yuan Wu, Nayan Singhal, and Philipp Krahenbuhl. Video compression through image interpolation. In *Proceedings of the European Conference on Computer Vision (ECCV)*, pages 416–431, 2018. 1, 2, 6, 7, 8

[36] Lei Zhou, Zhenhong Sun, Xiangji Wu, and Junmin Wu. End-to-end optimized image compression with attention mechanism. In *Proceedings of the IEEE Conference on Computer Vision and Pattern Recognition Workshops*, pages 0–0, 2019. 2